JOURNAL OF AIRCRAFT
Vol. 30, No. 2, March–April 1993

Stability Theory and Transition Prediction Applied to a General Aviation Fuselage

R. E. Spall*
University of South Alabama, Mobile, Alabama 36688
and
Y.-S. Wie†
High Technology Corporation, Hampton, Virginia 23666

The linear stability of a fully three-dimensional boundary layer formed over a general aviation fuselage was investigated. The location of the onset of transition was estimated using the *N*-factor method. The results were compared with existing experimental data and indicate *N*-factors of approximately 8.5 on the side of the fuselage and 3.0 near the top. Considerable crossflow existed along the side of the body, which significantly affected the unstable modes present in the boundary layer. Fair agreement was found between the predicted frequency range of linear instability modes and available experimental data concerning the spectral content of the boundary layer.

Nomenclature

H	=	total enthalpy
h_1, h_2	=	metric coefficients in the x and y coordinates, respectively
L	=	fuselage length, ft
l	=	length scale used in stability equations, taken as displacement thickness
Pr	=	Prandtl number, 0.72
R	=	Reynolds number, $U_e l/\nu_e$
Re_{cf}	=	crossflow Reynolds number, $U_n \delta_{0.1}/\nu_e$
s	=	arc length measured along y = const lines
$\hat{s}$	=	arc length for N-factor calculations
T_∞	=	freestream temperature, °R
U_e	=	edge velocity in $\hat{x}$ direction; velocity scale for stability equations
U_n	=	maximum velocity in crossflow direction
U_∞	=	freestream velocity, ft/s
u, v, w	=	velocity components in x, y, z directions, respectively
$\hat{u}$, $\hat{v}$, $\hat{w}$, $\hat{p}$, $\hat{T}$	=	disturbance eigenfunctions
V	=	total velocity, $(u^2 + v^2 + 2uv \cos \varphi)^{1/2}$
V_e	=	inviscid edge velocity
X	=	axial distance measured from the nose
x, y, z	=	body-oriented coordinates
$\hat{x}$, $\hat{y}$	=	orthogonal surface coordinates used in stability calculations
α, β	=	components of disturbance wave number in x and y directions, respectively
$\delta_{0.995}$	=	boundary-layer thickness
ζ	=	transformed normal coordinate
θ	=	azimuthal angle 0 and π on windward and leeward plane of symmetry
μ	=	dynamic viscosity
ρ	=	density
φ	=	angle between x and y surface coordinates
ω_i	=	growth rate
ω_r	=	disturbance frequency

Received May 24, 1991; revision received Nov. 11, 1991; accepted for publication Dec. 16, 1991.

*Assistant Professor, Department of Mechanical Engineering, EGCB 212. Member AIAA.
†Research Scientist, 28 Research Dr. Member AIAA.

Introduction

THE ability to predict (using analytical tools) the location of boundary-layer transition over aircraft-type configurations is of great importance to designers interested in laminar flow control (LFC). The e^N method, first used by Smith and Gamberoni,[1] has proven to be fairly effective in consistently predicting the location of the onset of transition for simple geometries in low-disturbance environments. This method provides a correlation between the most amplified single normal mode and the experimental location of the onset of transition. A comprehensive summary of studies which provide correlations between the value of N and the onset of transition is given by Malik.[2] These values generally fall within the range of 8–12, although values as low as 4.2 and as high as 20.9 have been reported.

For the correlations summarized by Malik,[2] the boundary-layer computations have been restricted to two-dimensional or axisymmetric flows, or have employed simple three-dimensional mean flows (e.g., rotating disk, infinite swept-wing or tapered swept-wing with straight isobars). For example, the linear stability code COSAL[3] utilizes the mean flow for a swept-wing with the conical flow similarity transformation in the spanwise direction. Unfortunately, for flows over general wing configurations, and nearly all flows over fuselage-type bodies at incidence, the analysis of fully three-dimensional flowfields is required. Exceptions to the above restrictions include the works of Cebeci and Chen,[4] Spall and Malik,[5] and Woan et al.[6]

In this article the linear stability of a low-speed boundary layer formed over a Cessna TP303 fuselage forebody is investigated. Transition prediction using the e^N method is more difficult for three-dimensional boundary layers formed over fuselage configurations than for swept-wing boundary layers. This is due, in part, to the possibility of multiple crossflow reversals occurring (as a function of the circumferential location) and to the associated range of instability mechanisms that may be present. Often, the idealized classification of linear instability mechanisms into Tollmien Schlichting (TS) or crossflow instabilities (as is usually done for boundary layers formed over swept wings) is inappropriate.

For the present analysis, the inviscid potential flow was computed using the widely available Hess[7] potential flow code. The mean flow was computed by using a second-order accurate finite-difference code developed by Wie,[8] and described in the next section. This code employs a second-order

accurate predictor-corrector form of the Crank-Nicolson scheme[9] and is well-suited for three-dimensional boundary-layer calculations, including regions of reversed crossflow. The stability calculations were performed using a modified version of the linear stability code COSAL. The code has been modified to allow for the analysis of fully three-dimensional boundary layers. Note that body and wavefront curvature terms have not been included in the stability equations. Curvature effects may be of the same order as nonparallel effects and thus the stability results (in terms of N-factor correlations) may be misleading if one were to include these terms in the stability equations while neglecting the nonparallelism of the boundary layer.

In the results section, computed values of N are correlated with experimentally determined locations for the onset of transition given in the dissertation of Vijgen[10] and also appearing in the work of Vijgen and Holmes.[11] In addition, comparisons between the unstable frequency band determined from linear stability theory and experimental hot-film measurements[10] are made. (Note that as a prelude to the flight tests, several stages of smoothing of the forebody surface were performed in order to reduce surface imperfections;[10] this is essential in maximizing the extent of laminar flow.) To the authors' knowledge, the present work represents the only available correlation of the results of linear stability theory (utilizing fully three-dimensional boundary layers) with experimental data for the estimated location of transition onset for an actual aircraft forebody configuration.

Numerical Procedure

The three-dimensional boundary-layer equations for the compressible flow in a body-oriented coordinate system (see Fig. 1) may be written as

Continuity Equation

$$\frac{\partial}{\partial x}(\rho u h_2 \sin\varphi) + \frac{\partial}{\partial y}(\rho v h_1 \sin\varphi) + \frac{\partial}{\partial z}(\rho w h_1 h_2 \sin\varphi) = 0 \tag{1}$$

x-Momentum Equation

$$\frac{\rho u}{h_1}\frac{\partial u}{\partial x} + \frac{\rho v}{h_2}\frac{\partial u}{\partial y} + \rho w \frac{\partial u}{\partial z} - \rho u^2 K_1 \cot\varphi + \rho v^2 K_2 \csc\varphi + \rho u v K_{12} = -\frac{\csc^2\varphi}{h_1}\frac{\partial p}{\partial x} + \frac{\cot\varphi \csc\varphi}{h_2}\frac{\partial p}{\partial y} + \frac{\partial}{\partial z}\left(\mu \frac{\partial u}{\partial z}\right) \tag{2}$$

y-Momentum Equation

$$\frac{\rho u}{h_1}\frac{\partial v}{\partial x} + \frac{\rho v}{h_2}\frac{\partial v}{\partial y} + \rho w \frac{\partial v}{\partial z} - \rho v^2 K_2 \cot\varphi + \rho u^2 K_1 \csc\varphi + \rho u v K_{21} = \frac{\cot\varphi \csc\varphi}{h_1}\frac{\partial p}{\partial x} - \frac{\csc^2\varphi}{h_2}\frac{\partial p}{\partial y} + \frac{\partial}{\partial z}\left(\mu \frac{\partial v}{\partial z}\right) \tag{3}$$

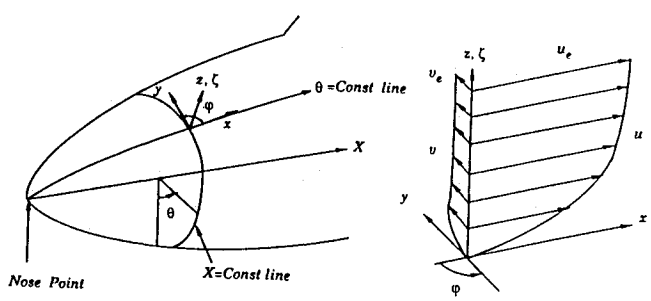

Fig. 1 Body-oriented coordinate system of the boundary-layer equations.

Energy Equation

$$\frac{\rho u}{h_1}\frac{\partial H}{\partial x} + \frac{\rho v}{h_2}\frac{\partial H}{\partial y} + \rho w \frac{\partial H}{\partial z} = \frac{\partial}{\partial z}\left[\frac{\mu}{Pr}\frac{\partial H}{\partial z} + \mu\left(1 - \frac{1}{Pr}\right)\frac{\partial}{\partial z}\left(\frac{V^2}{2}\right)\right] \tag{4}$$

The perfect gas equation and Sutherland's viscosity law are used to close the equation set. The metric coefficients h_1 and h_2 are functions of x and y. The parameters K_1 and K_2 are geodesic curvatures of the surfaces y = const and x = const, respectively, where

$$K_1 = \frac{1}{h_1 h_2 \sin\varphi}\left[\frac{\partial}{\partial x}(h_2 \cos\varphi) - \frac{\partial h_1}{\partial y}\right] \tag{5a}$$

$$K_2 = \frac{1}{h_1 h_2 \sin\varphi}\left[\frac{\partial}{\partial y}(h_1 \cos\varphi) - \frac{\partial h_2}{\partial x}\right] \tag{5b}$$

$$K_{12} = \frac{1}{h_1 h_2 \sin^2\varphi}\left[(1 + \cos^2\varphi)\frac{\partial h_1}{\partial y} - 2\cos\varphi \frac{\partial h_2}{\partial x}\right] \tag{5c}$$

$$K_{21} = \frac{1}{h_1 h_2 \sin^2\varphi}\left[(1 + \cos^2\varphi)\frac{\partial h_2}{\partial x} - 2\cos\varphi \frac{\partial h_1}{\partial y}\right] \tag{5d}$$

The boundary conditions are given as

$$z = \delta \quad u = u_e(x, y), \quad v = v_e(x, y), \quad H = H_e \tag{6a}$$

$$z = 0 \quad u = v = w = 0, \quad \left(\frac{\partial H}{\partial z}\right)_w = 0 \tag{6b}$$

For the windward and leeward symmetry planes v and K_1 $csc\varphi$ are zero and φ is generally $\pi/2$. Therefore, each term in the y-momentum equation vanishes. However, partial differentiation of Eq. (3) with respect to y yields an equation for $\partial v/\partial y$. The resulting equations for the planes of symmetry can be found in Ref. 8.

The boundary-layer edge conditions on v along the planes of symmetry are replaced with $\partial v/\partial y = \partial v_e/\partial y$, and in addition $\partial v/\partial y = 0$ at $z = 0$.

A Levy-Lees-type transformation is used to remove the singularity at $X = 0$. This transformation is of the form

$$x = x, \quad y = y, \quad \zeta = \sqrt{\frac{\rho_e u_e}{\mu_e s}}\int_0^z \frac{\rho}{\rho_e}\,dz \tag{7}$$

Matsuno's finite-difference scheme is used to march the solution downstream from the initial data plane. The method is a modification of the predictor-corrector form of the Crank-Nicolson scheme, which was originally suggested by Douglas and Jones[12] to apply to the three-dimensional boundary-layer problem. This scheme is half-implicit in the ζ direction, is explicit in the y direction, is noniterative and has second-order accuracy.[9] The unique character of this scheme is that the crosswise derivatives are formed independent of the sign of the crosswise velocity component. Matsuno's finite-difference scheme is conditionally stable,[9] and the stability condition gives the same constraint as that required by the zone of dependence principle.

The linear stability analysis of three-dimensional compressible boundary layers involves the solution of an eighth-order system of ordinary differential equations. The basic equations for the linear stability analysis of parallel-flow compressible boundary layers are derived using small disturbance theory. Infinitesimal disturbances of sinusoidal form are imposed on the steady boundary-layer flow and substituted into the compressible Navier-Stokes equations. Assuming that the mean flow is locally parallel, a

set of five ordinary differential equations is obtained. Of these, there are three second-order momentum equations, one second-order energy equation, and one first-order continuity equation. This system may be expressed as

$$\left(A\frac{d^2}{dz^2} + B\frac{d}{dz} + C\right)\hat{\Phi} = 0 \tag{8}$$

where $\hat{\Phi}$ is a five-element vector defined by $(\alpha\hat{u} + \beta\hat{v}, \hat{w}, \hat{p}, \hat{T}, \alpha\hat{v} - \beta\hat{u})$. The elements of the A, B, C matrices are given by Malik and Orszag.[13] The system is solved subject to the boundary conditions:

$$\Phi_1 = \Phi_2 = \Phi_4 = \Phi_5 = 0 \quad \text{at} \quad z = 0 \tag{9a}$$

$$\Phi_1, \Phi_2, \Phi_4, \Phi_5 \to 0 \quad \text{as} \quad z \to \infty \tag{9b}$$

In the computer code COSAL, a finite-difference method developed by Malik and Orszag[13] is incorporated for the solution of the compressible stability equations. This method employs a second-order accurate finite-difference formulation on a staggered grid, eliminating the need for pressure boundary conditions.

The above system provides, given the Reynolds number R, a complex dispersion relation of the form

$$\omega = \omega(\alpha, \beta) \tag{10}$$

For the temporal stability theory used in COSAL, α and β are real whereas ω is complex. Thus, it is assumed that the wave-like disturbances have $\hat{x}$ and $\hat{y}$ components of wave number α and β, respectively, and have a frequency $\omega_r = \mathrm{Re}(\omega)$. It is further assumed that the disturbances grow or decay only in time.

An N-factor for transition correlation may be defined as

$$N = \int_{\hat{s}_0}^{\hat{s}_t} \frac{\mathrm{Im}(\omega)}{|\mathrm{Re}(V_g)|}\, d\hat{s} \tag{11}$$

where $V_g = [(\partial\omega/\partial\alpha), (\partial\omega/\partial\beta)]$ is the complex group velocity and $\hat{s}$ is the arc length along an appropriate curve on the body surface. Subscripts 0 and t indicate critical and onset of transition, respectively.

The N-factor is not fully defined until a prescription is given for singling out a specific mode at each position on the body and for defining a specific curve along which to integrate. In COSAL, the integration is performed along the curve whose tangent is defined by the real part of the group velocity vector. In the present study, the individual modes are determined by maximizing the growth rate ω_i with respect to the disturbance wave numbers α and β (the "envelope method").

In the presentation of the results we discuss the wave orientation which is defined (with respect to the $\hat{x}$ axis) as

$$\Psi = \tan^{-1}(\beta/\alpha) \tag{12}$$

for a given location on the body. In dimensional terms the wavelength is given as

$$\lambda = \frac{2\pi l}{\sqrt{\alpha^2 + \beta^2}} \tag{13}$$

Results and Discussion

Results are presented for the linear stability of a low-speed boundary layer formed over a Cessna TP303 fuselage. N-factors are presented and correlated with experimental estimates of the onset of transition presented by Vijgen[10] and Vijgen and Holmes.[11] In addition, comparisons are made between the unstable frequency band determined from linear stability theory and those measured experimentally.[10] Stability calculations are performed for the conditions listed as test case 3 in the work of Vijgen.[10] This was an unpowered gliding flight test with one engine shut off and the other engine running at minimum idle power. The freestream velocity is given as $U_\infty = 279$ ft/s, and the freestream temperature as $T_\infty = 472°$R. These conditions (with Sutherlands viscosity law) result in a unit Reynolds number of 1.3 million/ft. The angle of attack is given as 0 deg. Although the angle of attack is zero, the body is not axisymmetric and regions of considerable crossflow develop. In the presentation of the results, the axial length measured along the centerline of the body (X), has been made nondimensional with respect to the Cessna fuselage length $L = 28.59$ ft.

The potential flow solution which is needed as input for the boundary-layer edge conditions was computed using the Hess code.[7] A description of the body with the paneling for the potential flow solution is shown in Fig. 2. The potential flow solution was obtained on a 54 × 37 grid (in the streamwise and circumferential directions, respectively). Due to the singularity of the panel method near the fuselage axis as $X \to 0$, the boundary-layer calculations are started slightly downstream from the fuselage nose.

The pressure coefficient resulting from the solution for the potential flow is plotted in Fig. 3. At the upper and lower symmetry lines, the pressure distribution is such that the velocity is directed towards the lines, i.e., both symmetry lines are inflow lines. The figure also indicates that a local maximum in the pressure distribution exists near $\theta = 125$ deg for $0 \le X/L \le 0.10$.

As previously noted, Matsuno's difference scheme is independent of the sign of the crossflow velocity, and thus the scheme is suitable for the solution of the boundary-layer equations even though the lower symmetry line is an inflow line. The boundary-layer solution was obtained using 300 points in the streamwise direction, with clustering toward the nose

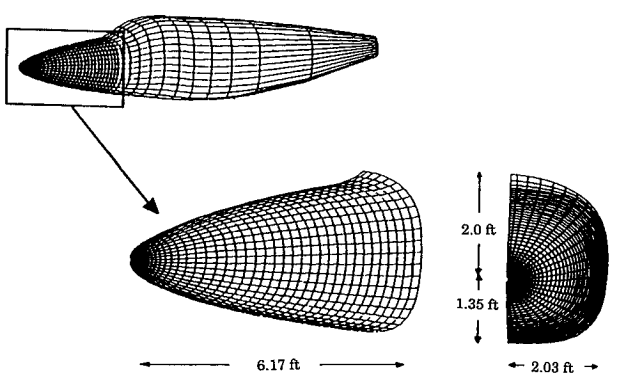

Fig. 2 Typical inviscid grid and fuselage description.

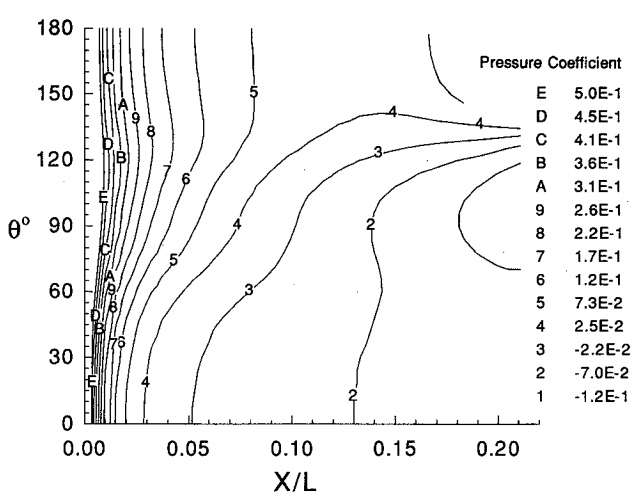

Fig. 3 Contours of constant pressure coefficient for flow over general aviation fuselage.

region, and 31 evenly spaced points in the circumferential direction. The grid spacing normal to the wall was $\Delta\zeta = 0.1$. The accuracy of the boundary-layer solution was examined by refining the grid in the wall-normal and circumferential directions, and the above distribution was found to be adequate for the stability analysis. Additional boundary-layer solutions for this configuration (with slightly different free-stream conditions) can be found in Wie and Harris.[14]

Figure 4 shows the distribution of the crossflow Reynolds number, defined as $Re_{cf} = U_n\delta_{0.1}/\nu_e$. Here, U_n is the maximum velocity in the crossflow direction and $\delta_{0.1}$ is the distance from the wall at which the crossflow decreases to 0.1 U_n. The maximum crossflow Reynolds number plotted is 200, although in the cross-hatched region the values are considerably higher. The value is limited to 200 in order to provide sufficient detail in the lower ranges. In addition, for low-speed flows, 200 represents an approximate upper limit for the crossflow Reynolds number for the existence of laminar flow. The most significant feature is the region centered about $\theta = 50°$ and $X/L = 0.07$ where $Re_{cf} > 125$. For low-speed flows this represents a significant level of crossflow which is likely to significantly alter the stability characteristics of the flow in this region. In addition, the relative value of crossflow Reynolds number to streamwise Reynolds number is significant in determining the stability characteristics of the boundary layer. That is, although Re_{cf} may remain large as the disturbance propagates in the streamwise direction, the ratio U_n/V_e (where V_e is the inviscid edge velocity) may decrease. This, in turn, shifts the most unstable modes from those characteristic of crossflow instabilities to those characteristic of TS instabilities.

The N-factors computed using linear stability theory are compared with the experimentally determined transition location as given by Vijgen[10] and Vijgen and Holmes.[11] A contour plot of the N-factors is given in Fig. 5. These contours were obtained from a series of calculations originating along neutral curves (for specific frequencies) at successive circumferential locations. Results for the frequencies which first reached $N = 9$ are plotted. These frequencies varied from 1000 Hz in regions of relatively high crossflow, to 1800 Hz in regions of relatively low crossflow. In addition, since the envelope method is used, the disturbances which are evaluated at each successive streamwise location (for a given dimensional frequency) represent the most unstable mode. Whether or not this corresponds to the evolution of an actual disturbance within a boundary layer is unknown. The experimental data points at streamwise locations indicating transitional flow are indicated on the contour plot. The detection of transition onset as well as the spectral content of the disturbances in the boundary layer was determined through surface hot-film anemometry.[10] The transition location was taken as that at which the turbulent intermittency level reached approximately 50%. The data point located along the side of the fuselage ($X/L = 0.111$, $\theta = 79$ deg) corresponds to a value of $N \approx 8.5$. This is in close agreement with previous correlations of other geometries in which N often falls in the range of 8–10. However, the data point near the top of the fuselage ($X/L = 0.093$, $\theta = 166.3$ deg) corresponds to a value of $N \approx 1.75$. This value is much lower than one would expect under conditions of a low disturbance environment if the surface of the body were free from roughness and waviness. Note that hot-film line II from Vijgen[10] follows closely along the constant contour $N = 9$ from $\theta \approx 54$ to $\theta \approx 79$ deg. It would be interesting to know if the forward movement of transition (near $\theta = 60$ deg) which is indicated from stability theory actually occurs on the aircraft. In this sense, stability theory may act as a useful guide in the placement of the hot-film sensors.

Vijgen and Holmes[11] also computed N-factors for this case using a streamwise axisymmetric analog method. This method is based on the assumption that the crossflow is small and can be neglected in the calculation of the boundary-layer profiles and in the subsequent stability analysis. Their results indicated that $N = 2.5$ at the transition point near the top of the fuselage and $N = 3.5$ at the point on the starboard side of the fuselage. The reasons for the differences between their values and those computed by analyzing the three-dimensional boundary layer are clear. The values given by Vijgen and Holmes indicate the highest N-factor found (over all possible frequencies) at the predetermined transition location. In the present case, a predetermined transition location was not assumed, instead, a value of $N = 9$ was used to estimate the location. Thus, the values of N upstream of the $N = 9$ contour level would actually be somewhat higher if the most unstable frequencies were determined for each contour level [i.e., the frequency that first results in $N = 2.5$ is different (higher) than the frequency that first results in $N = 9$]. In fact, for this point near the top of the fuselage a maximum of value of $N \approx 3.0$ was computed which resulted from a disturbance frequency of 1800 Hz. The value is slightly higher than that resulting from the axisymmetric analog method due to the nonzero levels of crossflow in the boundary layer. Unlike the analysis of two-dimensional/axisymmetric geometries, for fully three-dimensional flowfields it is impractical (in terms of the number of calculations necessary) to determine the maximum N-factors over the entire surface of the fuselage. The large discrepancy between value along the side is due to the crossflow in the boundary layer. As previously indicated, near the forward part of the fuselage along the side of the body, the crossflow Reynolds number reaches significant levels. The

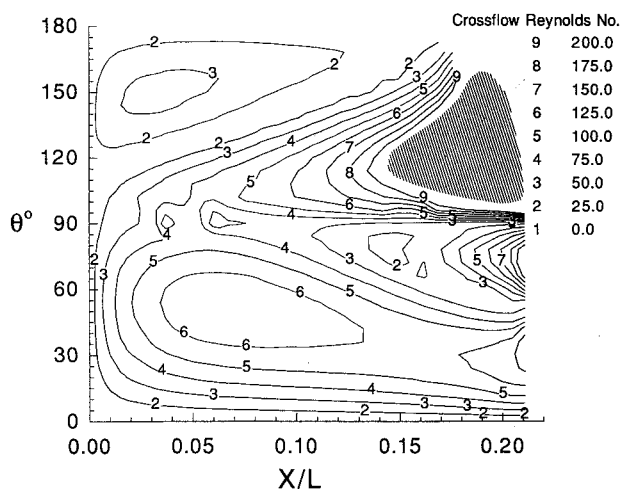

Fig. 4 Contours of constant crossflow Reynolds number. Contours above 200 have been omitted.

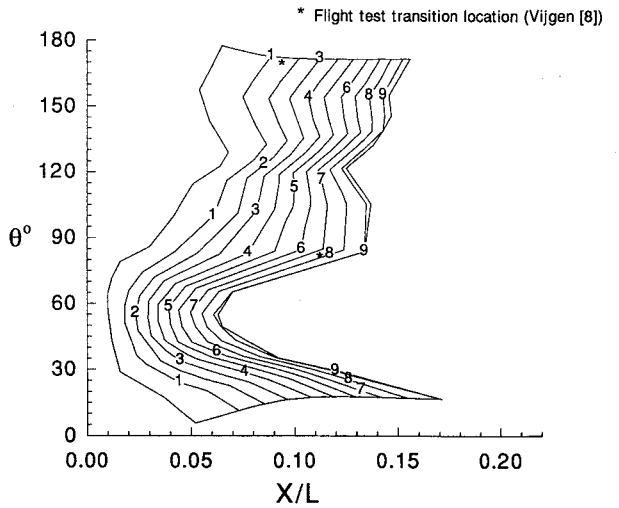

Fig. 5 Contours of constant N-factors, with * symbol indicating experimentally determined location of the onset of transition from Vijgen.[10]

axisymmetric analog method ignores this crossflow and thus underpredicts the growth rates of the most unstable modes within the boundary layer.

Figure 6 shows contours of constant temporal growth rate over the fuselage. These growth rates correspond to the modes followed in the plot of the N-factors, and thus do not indicate the highest growth rates within the boundary layer at any specific location, but represent the highest growth rates for a particular frequency, i.e., that frequency which first results in $N = 9$. The same is true for the plots of wavelength and wave angle that follow. It is clear that the region of high crossflow, as indicated in Fig. 4, corresponds to a localized region of high growth rates. Thus, in this region the influence of crossflow on the amplification rates is significant and should be accounted for.

Contours of constant wavelength (corresponding to N-factors given in Fig. 5) are shown in Fig. 7. The wavelengths have been nondimensionalized with respect to the boundary-layer thickness $\delta_{0.995}$. Typically, the (nondimensional) wavelengths associated with crossflow disturbances are on the order of 4–5. For TS disturbances, this increases to approximately 10–12. Thus we can identify, to some extent, the most unstable modes that may exist in the boundary layer. Note that near the top portion of the fuselage, the wavelengths range from 9–11. This indicates that TS type instabilities dominate, which may also be inferred from the plot of crossflow Reynolds number (Fig. 4). Along the sides of the body, and especially near the neutral curve the wavelengths are much lower. This indicates the importance that crossflow has on the stability of the boundary layer. As the disturbances evolve in the streamwise direction, the wavelengths of the most unstable disturbances increase, indicating the increasing importance of the viscous TS instability relative to the inviscid crossflow instability. This occurs because the ratio of U_n/V_e diminishes in the streamwise direction.

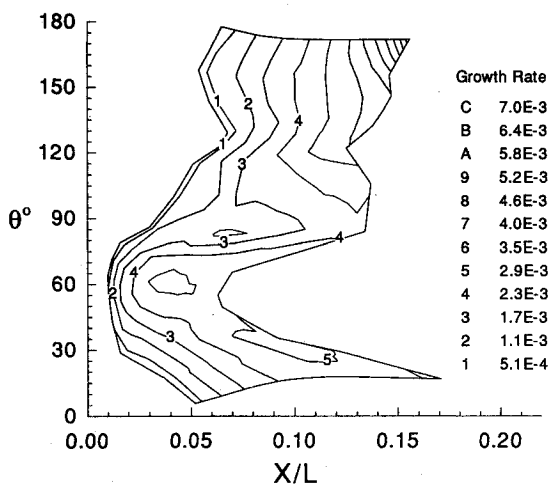

Fig. 6 Contours of constant temporal growth rate for frequencies which first result in $N = 9$.

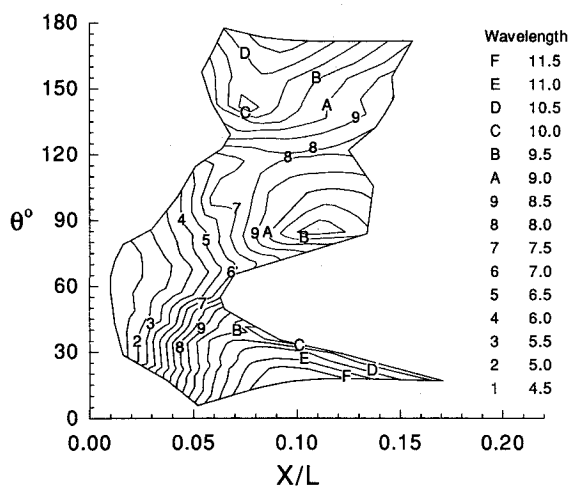

Fig. 7 Contours of constant wavelength (normalized by $\delta_{0.995}$) for disturbances resulting in N-factors given in Fig. 5.

The wave angle may also be used to gain information regarding the type of instability present in the boundary layer. Figure 8 shows that the wave angle (plotted with respect to the direction of the inviscid edge velocity) near the top portion of the fuselage changes from -40 to 0 deg as the disturbances evolve in the streamwise direction. This indicates that the crossflow influences the most unstable modes near the neutral point and that this influence decreases as the disturbance propagates in the streamwise direction. Over the lower portion of the body the wave angle is everywhere positive. This change in sign of the wave angle of the most unstable disturbances is due to the change in the direction of the inviscid edge velocity. This results in an immediate reversal of the crossflow at the body surface, which in turn shifts the direction of the most unstable wave angle. Similar results have also been reported for the case of a prolate spheroid at 10 deg incidence, for which regions of reversed crossflow develop.[5] The relatively high wave angles that exist over the mid and lower sections of the fuselage again indicate the importance of crossflow within the boundary layer.

Vijgen[10] performed a spectral analysis of hot-film signals at selected points along the top and side of the fuselage. The power spectra were determined using an FFT algorithm. The results can be used to quantify the dominant instabilities present in the boundary layer. Figures 9a–c show computed amplification rates and wave angles (as a function of frequency) corresponding to the most unstable linear disturbances, at locations corresponding to hot-film elements 21, 22, and 23, respectively. Note that element 21 ($X/L = 0.076$, $\theta = 65$ deg) is along the starboard side, and the experimental measurements were made with the starboard engine at idle (portside engine shutdown).[10] Thus, the propeller disturbance spectrum appeared in the hot-film signal. Elements 22 ($X/L = 0.085$, $\theta = 70$ deg) and 23 ($X/L = 0.093$, $\theta = 73$ deg) were also along the starboard side, but for these measurements, the starboard engine was shut down (portside engine at idle). As shown in Fig. 9a, linear stability predicts disturbance amplitude peaks at ≈600 Hz and ≈2200 Hz, with a local minimum at ≈1400 Hz. The experimental measurements indicated elevated energy levels in the range of 3500 Hz, and possibly below 1000 Hz. A minimum in the energy level occurred at ≈1500 Hz. The question is whether or not the elevated energy levels correspond to the presence of crossflow (lower frequency) and TS (higher frequency) disturbances in the boundary layer. The disturbance spectrum at lower fre-

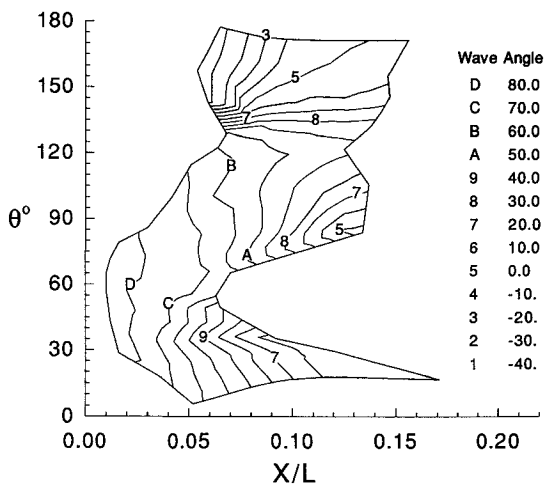

Fig. 8 Contours of constant wave angle.

quencies is consistent with predictions from linear theory. At higher frequencies the power spectral density (PSD) results reveal that the energy is distributed at frequencies which, according to linear theory, are stable. This shift in the frequency band could be explained if, e.g., the computed boundary-layer thickness were greater than the actual boundary-layer thickness. In addition, from Fig. 5 we see that at this

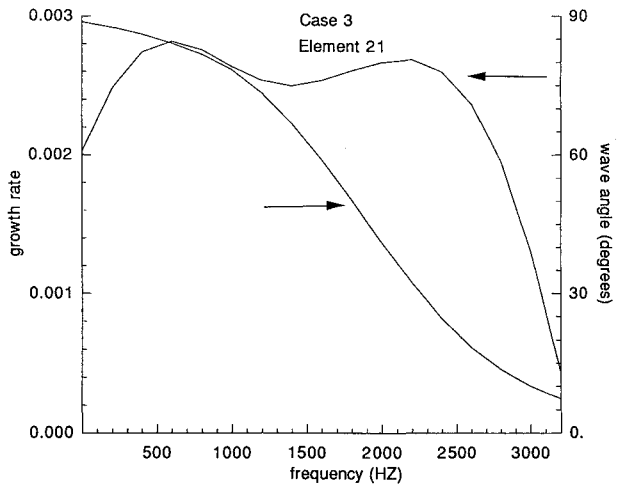

a) Corresponds to location of surface element 21[10]

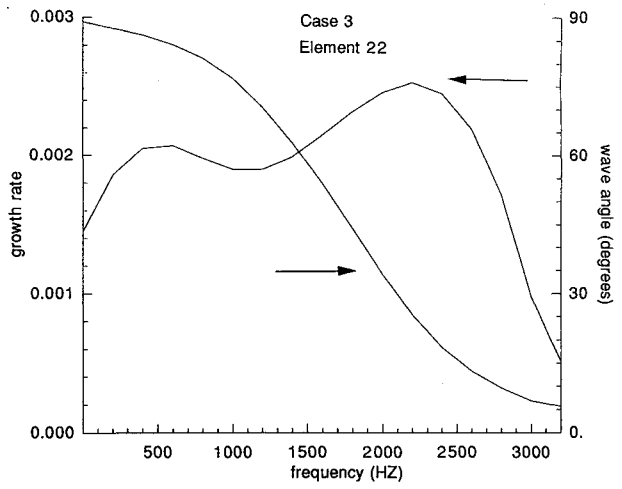

b) Corresponds to location of surface element 22

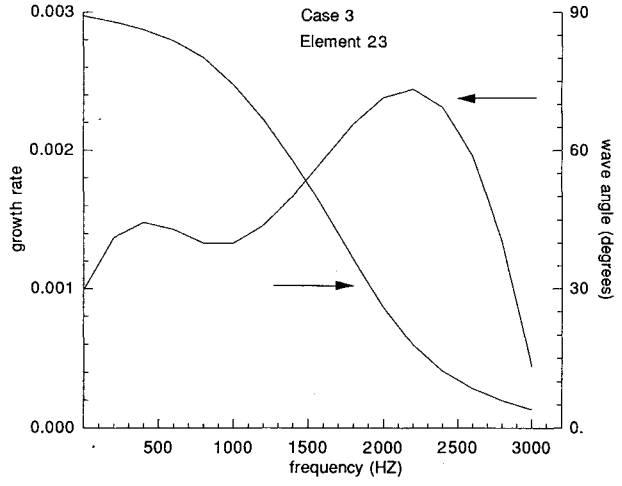

c) Corresponds to location of surface element 23

Fig. 9 Most amplified growth rate and corresponding wave angle as a function of frequency at three locations on fuselage forebody.

location $N \approx 9$. Thus, the disturbance growth may no longer be governed by set of linear equations. The wave angle of the most unstable disturbance at element 21 varies from ≈89 deg at $f = 0$ Hz to ≈12 deg at $f = 3200$ Hz. This variation is quite smooth and indicates the existence of a continuous spectrum of disturbances, ranging from highly oblique, stationary crossflow disturbances to (nearly) two-dimensional TS disturbances. We also note that the most amplified disturbances are intermediate between the highly oblique crossflow modes and the two-dimensional modes.

The computed stability results at elements 22 and 23 (shown in Figs. 9b and 9c, respectively) reveal that the maximum amplitudes of the lower frequency disturbances have decreased considerably. A slight decrease is also observed at the higher frequencies. This is due to a decrease in the crossflow Reynolds number which (as shown on Fig. 4) decreases from ≈125 to ≈90 in moving from element 21 to 23. This is accompanied by a slight drop in the wave angles at the higher frequencies, indicating that these nearly two-dimensional disturbances are also affected by crossflow in the boundary layer. The PSD distributions for elements 22 and 23,[10] reveal contradictory trends. At element 22, elevated energy levels were observed at frequencies below 1000 Hz, whereas at element 23 elevated energy levels appeared for frequencies above 3000 Hz. As mentioned previously, the linear stability theory reveals the existence of amplified disturbances at these locations, which at lower frequencies are characteristic of crossflow instabilities, and which at higher frequencies are characteristic of TS instabilities.

Conclusions

This article considered the linear stability of the three-dimensional boundary layer formed over a general aviation fuselage. Resulting N-factor calculations were compared with available experimental data for the location of the onset of transition. Results indicate that $N \approx 8.5$ along the side of the body and $N \approx 3.0$ along the top of the body. As discussed by Vijgen[10] surface waviness may have contributed to the low values of N along the top. Frequencies at which elevated energy levels were shown to exist in the boundary layer through spectral analysis of hot-film signals[10] showed only fair agreement with frequencies predicted using linear stability theory. In terms of the stability calculations these differences may have been due to influences such as body and wavefront curvature and nonparallel effects. Additional improvements between theory and experiment may be achieved by using an interactive technique in the computation of the boundary layer. In terms of the experimental results given by Vijgen,[10] early transition may have been triggered by effects such as surface irregularities, surface vibration, and other environmental disturbances. Of course, none of these effects are included in the present stability theory, and therefore the results of the study emphasize the need for caution when applying correlation methods such as e^N to real-design problems. It seems unlikely that stability analysis will ever be able to handle such surface irregularities in a completely general manner due to the difficulty associated with computing accurate mean flows. For detailed information regarding allowable manufacturing tolerances for laminar flow airframe surfaces, the reader is referred to an article by Holmes et al.[15]

Acknowledgments

The authors acknowledge support under contract NAS1-18240 from NASA Langley Research Center, Hampton, VA. The authors acknowledge M. R. Malik for his insightful comments on this topic.

References

[1]Smith, A. M. O., and Gamberoni, N., "Transition, Pressure Gradient, and Stability Theory," Douglas Aircraft Co., Rept. ES 26388, El Segundo, CA, Aug. 1956.

[2]Malik, M. R., "Stability Theory for Laminar Flow Control De-

sign," Progress in Astronautics and Aeronautics, Vol. 123, AIAA, Washington, DC, 1990, pp. 3–46.

[3]Malik, M. R., "COSAL–A Black Box Compressible Stability Analysis Code for Transition Prediction in Three-Dimensional Boundary Layers," NASA CR-165925, May 1982.

[4]Cebeci, T., and Chen, H. H., "Prediction of Transition on Airfoils with Separation Bubbles, Swept Wings and Bodies of Revolution at Incidence," Symposium on Numerical and Physical Aspects of Aerodynamic Flows, Long Beach, CA, Jan. 16–19, 1989.

[5]Spall, R. E., and Malik, M. R., "The Linear Stability of Three-Dimensional Boundary-Layers over Axisymmetric Bodies at Incidence," AIAA Paper 91-1640, Honolulu, HI, June 1991.

[6]Woan, C. J., Gingrich, P. B., and George, M. W., "CFD Validation of a Supersonic Laminar Flow Control Concept," AIAA Paper 91-0188, Reno, NV, Jan. 1991.

[7]Hess, J. L., "Calculation of Potential Flow About Arbitrary 3-D Lifting Bodies," Rept. MDC J5679-01, Douglas Aircraft Co., Long Beach, CA, Oct. 1972, available from Defense Technology Information Center as AD 755 480.

[8]Wie, Y.-S., "A Three-Dimensional, Compressible, Laminar Boundary-Layer Method for General Fuselages," NASA CR-4292, Vol. 1, May 1990.

[9]Matsuno, K., "A Vector-Oriented Finite-Difference Scheme for Calculating Three-Dimensional Compressible Laminar and Turbulent Boundary Layers on Practical Wing Configurations," AIAA Paper 81-1020, Palo Alto, CA, June 1981.

[10]Vijgen, P., "Incompressible Boundary-Layer Transition Flight Experiments over a Nonaxisymmetric Fuselage Forebody and Comparisons with Laminar Boundary-Layer Stability Theory," Ph.D. Dissertation, Univ. of Kansas, Dept. of Aerospace Engineering, Lawrence, KS, Dec. 1988.

[11]Vijgen, P., and Holmes, B. J., "In-Flight Transition Measurements on a Non-Axisymmetric Fuselage Forebody and Correlation with Boundary-Layer Stability Theory," SAE TP 881395, Oct. 1988.

[12]Douglas, J., Jr., and Jones, B. F., "On Predictor-Corrector Methods for Nonlinear Parabolic Differential Equations," *Society of Industrial Applied Math Journal*, Vol. 11, No. 1, 1963, pp. 195–204.

[13]Malik, M. R., and Orszag, S. A., "Efficient Computation of the Stability of Three-Dimensional Compressible Boundary-Layers," AIAA Paper 81-1277, Palo Alto, CA, June 1981.

[14]Wie, Y.-S., and Harris, J. E., "Numerical Solution of the Boundary-Layer Equations for a General Aviation Fuselage," AIAA Paper 90-0305, Reno, NV, Jan. 1990.

[15]Holmes, B. J., Obara, C. J., Martin, G. L., and Domack, C. S., "Manufacturing Tolerances for Natural Laminar Flow Airframe Surfaces," SAE Paper 850863, Wichita, KS, April 1985.